INTERNATIONAL JOURNAL OF HYDROGEN ENERGY 36 (2011) 13793–13807

Available at www.sciencedirect.com

ScienceDirect

journal homepage: www.elsevier.com/locate/he

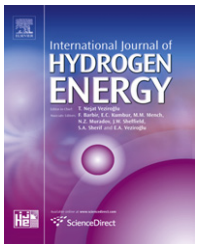

Multidimensional CFD simulation of syngas combustion in a micro-pilot-ignited dual-fuel engine using a constructed chemical kinetics mechanism

Ulugbek Azimov, Masahiro Okuno, Kazuya Tsuboi [1], Nobuyuki Kawahara [2], Eiji Tomita [3]*

Department of Mechanical Engineering, Okayama University, 3-1-1 Tsushima-naka, Kita-ku, Okayama 700-8530, Japan

ARTICLE INFO

Article history:
Received 8 June 2011
Received in revised form
29 July 2011
Accepted 30 July 2011
Available online 25 August 2011

Keywords:
Dual-fuel engine
Syngas combustion
Chemical kinetics mechanism
CFD simulation

ABSTRACT

A multidimensional computational fluid dynamics (CFD) simulation of a constructed syngas chemical kinetic mechanism was performed to evaluate the combustion of syngas in a supercharged dual-fuel engine for various syngas initial compositions under lean conditions. The modelled results were validated by comparing predictions against corresponding experimental data for a supercharged dual-fuel engine. The predicted and measured in-cylinder pressure, temperature, and rate of heat release (ROHR) data were in good agreement. The effect of the hydrogen peroxide chain-propagation reaction on the progress of combustion under supercharged conditions was examined for different types of syngas using various initial H_2 concentrations. The effect of the main syngas kinetic mechanism reactions on the combustion progress was analysed in terms of their contribution to the total heat of the reaction. The best results compared with experimental data were obtained in the range of equivalence ratios below about 0.8 for all types of syngas considered in this paper. As the equivalence ratio increased above 0.8, the results deviated from the experiment data. The spatial distribution of the in-cylinder temperature and OH* within this equivalence-ratio range showed the completeness of the combustion. The present CFD model captured the overall combustion process well and could be further developed into a useful tool for syngas-engine combustion simulations.

1. Introduction

Advanced power systems that are projected to achieve high efficiency and low emissions rely on synthesis gas (syngas) as a key intermediate energy carrier [1]. In such systems, biomass or coal is converted to syngas via gasification or partial oxidation [2]. Syngas consists of combustible gases composed of mainly carbon monoxide (CO), hydrogen (H_2), and methane (CH_4), and non-combustible gases composed of mainly nitrogen (N_2), carbon dioxide (CO_2) and water vapour (H_2O). Varying proportions of H_2, CO, CH_4, CO_2, H_2O, and N_2 may be present [3]. Advanced reciprocating engines are considered a potential means of converting syngas into power because of their role in distributed energy (DE) production and

* *Corresponding author*. Tel.: +81 86 251 8049; fax: +81 86 251 8266.
E-mail addresses: uazimov2001@yahoo.com (U. Azimov), gen421109@s.okayama-u.ac.jp (M. Okuno), tsuboi@mech.okayama-u.ac.jp (K. Tsuboi), kawahara@mech.okayama-u.ac.jp (N. Kawahara), tomita@mech.okayama-u.ac.jp (E. Tomita).
[1] Tel.: +81 86 251 8238; fax: +81 86 251 8266.
[2] Tel.: +81 86 251 8235; fax: +81 86 251 8266.
[3] Tel.: +81 86 251 8049; fax: +81 86 251 8266.

0360-3199/$ – see front matter
doi:10.1016/j.ijhydene.2011.07.140

Nomenclature

c_p	specific heat capacity, J/kg K
y^+	dimensionless normal distance from the wall for hydrodynamic boundary layer, –
y_T^+	dimensionless normal distance from the wall for thermal boundary layer, –
Pr	molecular Prandtl number, –
Pr_{tr}	turbulent Prandtl number, –
u	tangential fluid velocity, m/s
u_w	tangential wall velocity, m/s
u^+	dimensionless velocity, –
P	sublayer resistance factor, –
ρ	density, kg/m^3
u_τ	wall shear stress, kg/m s^2
T^+	dimensionless temperature, –
T_w	wall temperature, K
T	temperature, K
q_w	wall heat flux, W/m^2
κ	von Karman constant, 0.419
E	empirical coefficient, 0.9
k	turbulent kinetic energy, m^2/s^2
ε	turbulent dissipation rate, m^2/s^3
h_l	local heat-transfer coefficient, W/m^2 K
ϕ	equivalence ratio, –
θ_{inj}	injection timing, CA^0

their combination of high efficiency and low cost [4]. Mixtures of H_2 and CO have high antiknock behaviour and therefore could serve as fuels for internal-combustion engines [5,6]. However, the addition of H_2 to CO or CH_4 tends to increase combustion temperatures and nitric oxide (NO) emissions under stoichiometric conditions [7]. Therefore, such mixtures are more appropriate for lean-burn applications, where combustion temperatures are moderated by excess air.

The main benefit of utilizing syngas as a fuel for power generation is obtained when syngas is used in dual-fuel engines that operate under compression ignition with a lean mixture, using a pilot injection of diesel fuel [8]. Some fuels do not have sufficient ignition properties to enable ignition, so two fuels must be used. The ignition of the primary fuel (typically gaseous) is activated by the in-cylinder conditions. In this case, first, a pilot diesel fuel is injected, resulting in ignition and a subsequent temperature rise in the combustion chamber [9,10]. Then, the primary gaseous fuel, which in this case is syngas, is ignited as the chamber temperature increases, with subsequent combustion. Dual-fuel engines have been employed for a wide range of applications to utilize gaseous fuels. They are most commonly modified diesel engines and can achieve very low emission levels, particularly for smoke and particulates. The benefits of the dual-fuel conversion include smoother and quieter operation, significantly longer engine life between overhauls, fuel savings, and enhanced safety.

A few published works have described the use of syngas as a fuel for internal combustion (IC) engines. These include the work of Karim and coworkers [11,12] and McMillian and Lawson [13]. Bilcan [14] studied the use of various gaseous fuels, including syngas, in dual-fuel engines. Baratieri et al. [15] conducted a comparative analysis on the use of biomass-based syngas in internal-combustion (IC) engines and combined-cycle gas turbine (CCGT) plants. They concluded that the IC engine configuration is characterized by a significant thermal energy fraction that makes it possible to reach global energy efficiencies higher than 70%. Boehman and Le Corre [16] surveyed the published work on syngas combustion in reciprocating engines and focused on dual-fuel combustion in compression-ignition engines. Tomita et al. [17] investigated the combustion characteristics and performance of supercharged syngas with micro-pilot ignition in a dual-fuel engine. With a certain increase in syngas H_2 content, the engine was found to operate with stable combustion and high efficiency, even at an equivalence ratio of 0.45, because the increased hydrogen content enhanced the lean limit of the mixture. Roy et al. [18,19] studied the effect of H_2 content in the syngas produced from biomass and the effect of exhaust gas recirculation (EGR) in the syngas produced from H_2-rich coke oven gas on the performance and exhaust emissions of a dual-fuel engine. They found that the engine power with the high-H_2-content syngas increased by 12%, and that the high-H_2-content syngas was superior to the low-H_2-content gas for leaner operations.

Improvements made to the fuel flexibility of syngas-combustion technology by optimizing the combustion mechanism will provide for an increased acceptable range in the variation of fuel composition and conditions. Several research groups have recently developed chemical kinetics mechanisms to simulate syngas combustion. Yetter et al. [20] developed a comprehensive reaction mechanism for CO and H_2, which are considered the main combustible species in syngas. Saxena and Williams [21] tested a small detailed chemical kinetic mechanism for the combustion of H_2 and CO. They made a few revisions to the rate parameters for the elementary steps in the mechanism for H_2, deleted the H_2 initiation step, and added an initiation step for CO along with changes to the three-body recombination rates and chaperon efficiencies. They reported that with these changes, a reasonable agreement was obtained with measured burning velocities, diffusion-flame extinction conditions, and autoignition times. Frassoldati et al. [22,23] studied the combustion and flame structure of CO–H_2 mixtures. They developed a kinetic scheme for turbulent diffusion flames by coupling a kinetic postprocessor with a computational fluid dynamics (CFD) code to investigate the flame structure and pollutant formation. Liu and Karim [24] coupled H_2 chemical kinetics models with CFD and studied combustion characteristics of Homogeneous Charge Compression Ignition (HCCI) engine. Wang et al. [25] performed modelling study of Spark-Ignited (SI) engine fuelled with natural gas-H_2 mixtures by coupling CFD and detailed chemical kinetics and observed better accuracy for the case with detailed chemistry model than that with simple chemistry model. Slavinskaya et al. [26] developed a skeletal reaction mechanism for syngas combustion in gas turbines with 12 species and 20 irreversible reactions. This mechanism was validated for pressures up to 20 bars with

different mixture contents and fuel–air ratios. Starik et al. [27] developed a kinetic model that describes the processes of ignition and combustion of $CO–H_2–O_2–N_2$ mixtures. The model was validated over wide ranges of temperature, pressure, and equivalence ratio using experimental data for the ignition delay time and laminar-flame propagation velocity, and also for the evolution of the most important species. Sun et al. [28] studied high-pressure flame speeds and performed kinetic modelling of CO/H_2 combustion. The comparison between the modelled results and laboratory measurements suggested that the accuracy of the thermochemical data and the elementary rate constants is crucial for obtaining satisfactory performance of the reaction mechanism. Sivaramakrishnan et al. [29] studied the combustion of CO/H_2 mixtures at elevated pressures. They showed that the model they developed underpredicted CO and O_2 decay and CO_2 formation at very high pressures of 256 and 450 bars. They concluded that HO_2 radical reactions appear to be among the most sensitive reactions in the model under these conditions. Cavaliere et al. [30] modelled kinetically the ignition of syngas/air mixtures at low temperature and high pressure with the four reaction mechanisms described by Frassoldati et al. [22], Saxena and Williams [21], Yetter et al. [20], and GRI Mech 3.0 [31]. They found that for a mixture of CO and H_2, all mechanisms predicted the experimental data accurately for temperatures above 1000 K regardless of the pressure. But below this temperature, the simulation results deviated from the experimental data. Mittal et al. [32] used experiments with a rapid-compression machine and numerical studies to evaluate the combustion mechanism for CO/H_2 mixtures at high pressures in the range of 15–50 bars and at temperatures of 950–1100 K. Their results demonstrated that any evaluation of a kinetic scheme by reference to ignition delays must be treated with some caution when the kinetic uncertainties are not taken into account. Chaos and Dryer [33] reviewed the possibility of using gas turbine syngas combustion with higher pressures and lower temperatures to test the comprehensive nature of the existing detailed chemical kinetic models. They proposed kinetic changes to improve the predictions of syngas combustion under these conditions and emphasized that the higher pressure, lower-temperature conditions encountered in gas turbines point to the importance of and the need for further theoretical as well as experimental studies of elementary reactions involving HO_2 and H_2O_2 chemistry.

Although many numerical models of the combustion of conventional fuels in IC engines have been developed, very few modelling and simulation studies have been performed on syngas combustion in IC engines [34,35]. Papagiannakis et al. [34] studied the performance and exhaust emissions of an SI engine operating on syngas and developed a mathematical model to simulate its operation. In this model, combustion is initiated by a spark discharge, whereas the burning rate of syngas depends on its entrainment rate into the burning zone, which is controlled by the velocity of the flame front that is formed at the boundary of the burning zone spreading inside the combustion chamber. The concentration of each of the 11 species (H_2O, H_2, OH^*, H^*, N_2, NO, N, CO_2, CO, O_2, and O^*) that are considered to be in chemical equilibrium inside the burning zone was calculated by solving a system of 11 equations. Gamino and Aguillon [35] performed a numerical simulation of the syngas combustion process in an IC engine using a mathematical model that included balances for the conservation of mass and energy and reaction rates for different chemically reactive species in syngas. Three-step homogeneous reactions were used for the combustion process.

One limitation of the two approaches described above is that they are not able to accurately represent the interactions between turbulent fluid dynamics and chemical kinetics. These turbulence–chemistry interactions can have significant effects on flame stability and pollutant formation during engine combustion. It has been shown that the effects of turbulent mixing must be considered to obtain better agreement with experiments during the combustion phase [36]. There is an urgent need for a reliable engine-simulation model that represents the turbulence–chemistry interactions by combining CFD and a syngas chemical kinetics mechanism. This model will help predict the combustion behaviour of syngas with various chemical compositions from different feedstock, such as biomass, coal, and refinery residues, as a necessary precondition for establishing numerical tools to verify system designs at early developmental stages.

Therefore, the objective of this study was to simulate dual-fuel engine syngas combustion under lean conditions by coupling a validated turbulence model available in a CFD code with a constructed syngas chemical kinetics mechanism.

2. Experimental and numerical setup

In this study, simulations were performed on the combustion in a water-cooled four-stroke single-cylinder engine with two intake and two exhaust valves, described in detail in Ref. [18]. In this engine, the autoignition of a small quantity of diesel pilot fuel, injected into the combustion chamber before top dead centre (TDC), initiates the combustion. The burning diesel fuel then ignites the gaseous fuel. A commercial solenoid-type injector that is typically used for diesel-only operations was modified to ensure that only a small quantity of fuel was injected. The seven-hole nozzle of the commercial injector was replaced by one with four holes, 0.1 mm in diameter. The diesel fuel injection timing and duration were controlled through signals transferred to the injector from the injector driver. A common-rail injection system was employed to supply a constant injection pressure of 80 MPa to the injector. The quantity of injected pilot diesel fuel was 1.2 mg/cycle.

A zero-dimensional kinetic analysis was performed using the CHEMKIN code with a single-zone model under HCCI conditions without taking into account turbulence. The intake-valve closure (IVC) time was 135 crank-angle degrees (CA°) before top dead centre (BTDC), and the simulation was run for 265 CA°. The gas mixture composition at IVC varied according to syngas type and equivalence ratio. For example, for syngas Type 1 and equivalence ratio 0.63 the gas mixture composition at IVC was (in mass fraction): CH_4 – 0.04074, CO – 0.083670, CO_2 – 0.099053, H_2 – 0.003672, O_2 – 0.134309, N_2 – 0.675223. The gas mixture pressure and temperature at IVC were 225 kPa and 450 K, respectively. Then,

Table 1 – Engine specification and simulation conditions.

Engine type	4-stroke, single-cylinder water-cooled
Bore × stroke	96 × 108 mm
Swept volume	781.7 cm^3
Compression ratio	16
Combustion system	Dual-fuel, direct injection
Combustion chamber	Shallow dish
Engine speed	1000 rpm
Intake valve closure (IVC)	135 deg. BTDC
Initial pressure at IVC	225 kPa
Initial temperature at IVC	330 K
Injection system	Common-rail
Nozzle hole × diameter	4 × 0.10 mm
Pilot fuel injection pressure	80 MPa
Pilot fuel injection quantity	1.2 mg/cycle
Equivalence ratio	Variable

a multidimensional CFD analysis was performed using the Star-CD V4.0 code. The simulations began from the intake-valve closure at 135° CA BTDC and were carried until 130° CA after top dead centre (ATDC). The simulation conditions with the engine specifications and different types of syngas compositions used in this study are given in Tables 1 and 2, respectively.

This version of Star-CD incorporates the CHEMKIN code to formulate the gas-phase chemistry with an advanced solver approach. The Star-CD code provides CHEMKIN with the thermodynamic information for the computational cells, and the CHEMKIN code returns the new species information after solving the chemistry. After solutions are obtained for all cells, the mass transfer, heat transfer, and flow between cells are simulated by the corresponding sub-models. Then, the interactions between the turbulent mixing and the chemical reactions are implemented.

The CFD model was based on the Reynolds-averaged governing equations; it was set to account for turbulence, the liquid fuel-injection spray, and chemical mechanisms and was used the experimental conditions. The standard high-Reynolds number k–ε model was used for the turbulence modelling. The well-justified assumptions were applied that an entire cylinder wall, cylinder head and piston surface is at constant temperature. Constant temperature of 450 K was used for the cylinder wall and cylinder head, and 500 K was used for the piston surface. Heat transfer by conduction through the cylinder wall is one dimensional. The properties of the cylinder wall remain constant with temperature and time. The wall heat-transfer model was represented as a standard wall function:

$$T^+ = \begin{cases} \mathrm{Pr}y^+ & , \quad y^+ \le y_T^+ \\ \mathrm{Pr}_{tr}(u^+ + P) & , \quad y^+ > y_T^+ \end{cases}, \tag{1}$$

where y^+ is the dimensionless normal distance from the wall, $u^+ = (u - u_w)/u_\tau$, where, u – tangential fluid velocity, u_w – tangential wall velocity, $u_\tau = (\tau/\rho)^{1/2}$ – wall shear stress, P is the sublayer resistance factor.

$$P = 9.24\left[\left(\frac{\mathrm{Pr}}{\mathrm{Pr}_{tr}}\right)^{3/4} - 1\right]\left[1 + 0.28\exp\left(\frac{-0.007\mathrm{Pr}}{\mathrm{Pr}_{tr}}\right)\right], \tag{2}$$

$T^+ = c_p\rho(T_w - T)u_\tau/q_w$, where, T_w is the wall temperature, Pr is the molecular Prandtl number, Pr_{tr} is the turbulent Prandtl number, and q_w is the heat flux. Here, y_T^+ satisfies the equation

$$\mathrm{Pr}y_T^+ - \mathrm{Pr}_{tr}\left[\frac{1}{\kappa}\ln\left(Ey_T^+\right) + P\right] = 0 \tag{3}$$

where, E – empirical coefficient, 0.9; κ – von Karman constant, 0.419.

The local heat-transfer coefficient is

$$h_l = \frac{q_w}{T_w - T} = \frac{c_p\rho u_\tau}{\mathrm{Pr}_{tr}\,(u^+ + P)} \tag{4}$$

where, c_p – heat capacity, ρ – density,

The pressure-implicit split-operator (PISO) algorithm was used to simulate the transient flow of the engine. The injection process included the flow in the nozzle hole and the atomisation process. The properties of atomisation and secondary breakup were calculated by the Reitz–Diwakar model [37,38]. To reduce the computation time, a 90° moving-sector mesh of 7296 cells with cyclic boundaries was used to represent a bowl-in-piston configuration that was representative of the experimental single-cylinder pilot-ignited dual-fuel engine [18]. The mesh pattern and the cell-size distribution within the computation domain of the full mesh were different from those of the sector mesh. The sensitivity of the grid was validated by comparing the motoring in-cylinder pressure histories from experiments using both a full-mesh simulation and a sector-mesh simulation. Fig. 1 shows that the motoring in-cylinder pressure predicted by the sector-mesh simulation precisely matched the values obtained from the experiment and the full-mesh simulation. A grid size between 0.5 and 2.0 mm and a time step of 0.1° CA provided good numerical accuracies and computation stabilities.

3. Construction of the syngas kinetics mechanism

Four mechanisms were constructed to evaluate the in-cylinder pressure during dual-fuel engine combustion and to validate the simulation results with experimental data. The list of the kinetic mechanisms used in this study is given in Table 3. All mechanisms were constructed from the nine-step reduced mechanism for CH_4 autoignition by Li et al. [39]. This was combined with various detailed mechanisms; any resulting duplicate reactions were eliminated from the Li et al. mechanism. Mechanism 1 used a H_2/CO detailed mechanism by Saxena and Williams [21], eliminating $HCO + O_2 \Leftrightarrow CO + HO_2$, $HCO(+M) \Leftrightarrow CO + H^*(+M)$, $H^* + O_2(+M) \Rightarrow HO_2(+M)$, and $H_2O_2(+M) \Leftrightarrow OH^* + OH^*(+M)$. Mechanism 2 used a skeletal mechanism for syngas combustion developed by Slavinskaya et al. [26], eliminating $HCO + O_2 \Leftrightarrow CO + HO_2$, $HCO(+M) \Leftrightarrow CO + H^*(+M)$, and $H^* + O_2(+M) \Rightarrow HO_2(+M)$. Mechanism 3 used a detailed mechanism for H_2/CO/O_2 combustion developed by Frassoldati et al. [22], eliminating $HCO + O_2 \Leftrightarrow CO + HO_2$, $HCO(+M) \Leftrightarrow CO + H^*(+M)$, $H^* + O_2(+M) \Rightarrow HO_2(+M)$, and $H_2O_2(+M) \Leftrightarrow OH^* + OH^*(+M)$. Mechanism 4 used the reduced 9-step mechanism for H_2 combustion by Fernandez–Galisteo et al. [40], which includes the H_2–O_2 chain, direct recombination, and HO_2 reactions, and

Table 2 – Syngas composition.

Gas type	Composition					LHV (MJ/kg)	Source
	H2 (%)	CO (%)	CH4 (%)	CO2 (%)	N2 (%)		
Type 1	13.7	22.3	1.9	16.8	45.3	4.13	BMG
Type 2	20.0	22.3	1.9	16.8	39.0	4.99	BMG
Type 3	13.7	22.3	1.9	23.0	39.1	3.98	BMG
Type 4	56.8	5.9	29.5	2.2	5.6	38.69	COG

the detailed mechanism for $H_2/CO/O_2$ combustion developed by Frassoldati et al. [22].

To simulate the pilot-injected diesel spray and ignition, the chemistry of n-heptane (C_7H_{16}) was included in the constructed mechanisms as a single-step reaction, $C_7H_{16} + 11O_2 \Leftrightarrow 7CO_2 + 8H_2O$, based on an eddy breakup (EBU) mixing representation by specifying the EBU reaction parameters [41]. Previous studies have shown that for conventional diesel combustion, both diesel and C_7H_{16} fuels show a similar ROHR [42]. This implies that C_7H_{16} is only used to initiate the pilot ignition of syngas. After the syngas is ignited, the combustion proceeds without any C_7H_{16} chemistry. The reason for this simplification is that the amount of injected diesel fuel was 1.2 mg/cycle, which provides only 2% of the total energy value in the cylinder, with negligible contribution to the total ROHR. Previous results [18,19] have shown that when micro-pilot injection is used, the ROHR profiles do not include any changes due to the pilot diesel fuel combustion, which is opposite to what has been found when the amount of pilot-injected fuel is high, as in Ref. [16]. Additionally, the experimental results showed an undetectable level of smoke during micro-pilot diesel fuel combustion.

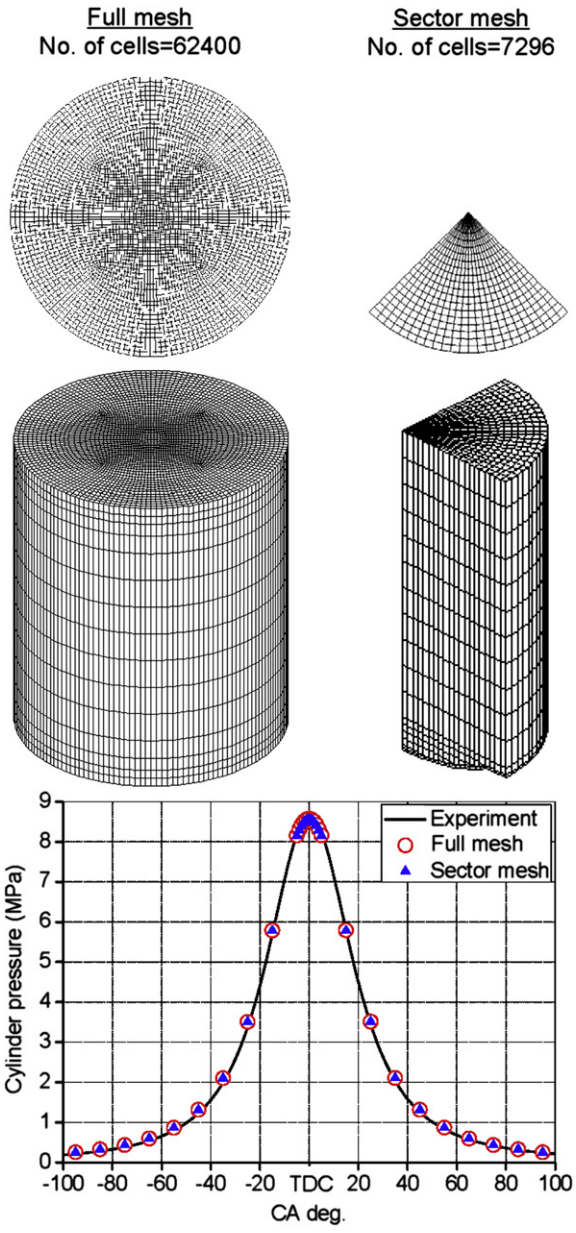

Fig. 1 – Computation mesh and motoring in-cylinder pressure.

Constructed mechanism 3 was selected for our variable-volume chemical kinetics calculations, which reproduced the compression and expansion strokes, thereby assuming a homogeneous zero-dimensional adiabatic model of the internal-combustion engine. The constructed reduced syngas mechanism 4 was used for the CFD simulations. These mechanisms do not include NO_x chemistry; however, in future studies, the NO_x chemistry mechanism can easily be incorporated into the constructed mechanisms.

In premixed flames at low or atmospheric pressures that are low enough for the third explosion limit of H_2, the hydrogen peroxide (H_2O_2) chemistry is not important at a first approximation. These reactions can be neglected at lower pressures, although some studies have reported a syngas combustion mechanism that excluded these reactions even at higher pressures under gas turbine conditions [26]. However, during combustion at supercharged engine conditions, reactions with the formation and consumption of H_2O_2 become especially important. When the pressure nears the third limit of hydrogen ignition, the diffusion of HO_2 radicals towards the walls becomes more difficult, and this could result in bimolecular reactions forming H_2O_2, which can decompose into two very reactive OH^* radicals. Moreover, the importance of these reactions changes with the equivalence ratio. Fernandez–Galisteo et al. [43] showed that at the third H_2 explosion limit above about 1 MPa, H_2O_2 becomes an important intermediate radical generator. The effect of the H_2O_2 chemistry under higher pressures will be discussed in subsequent sections.

Previous research has highlighted the relative importance of selected elementary reactions that most significantly affect the ROHR in a rapid-compression machine at specific reaction

Table 3 – Chemical kinetics mechanisms used in this study.

No.	Mechanism	No. species	No. reactions
1	Reduced mechanism for CH4 by Li et al. [39] + Detail mechanism for H2/CO by Saxena et al. [21]	16	35
2	Reduced mechanism for CH4 by Li et al. [39] + Skeleton mechanism for Syngas by Slavinskaya et al. [26]	16	26
3	Reduced mechanism for CH4 by Li et al. [39] + Detail mechanism for H2/CO by Frassoldati et al. [22]	16	39
4	Reduced mechanism for CH4 by Li et al. [39] + Reduced mechanism for H2 by Fernandez-Galisteo et al. [40] + Detail mechanism for CO/CO2 by Frassoldati et al. [22]	16	29
5	Detail mechanism GRI Mech 3.0 [31]	53	325

times following the end of the compression stroke, measured in terms of the participation index [44]. The most important selected reactions at high pressures are listed below.

Chain-initiation reactions

$$CH_4 + O_2 \Leftrightarrow CH_3 + HO_2 \quad (R1)$$

$$CO + HO_2 \Leftrightarrow CO_2 + OH^* \quad (R2)$$

Chain-propagation reactions

$$H_2O_2 + H^* \Leftrightarrow H_2 + HO_2 \quad (R3)$$

$$H_2O_2(+M) \Leftrightarrow OH^* + OH^*(+M) \quad (R4)$$

Chain-branching reactions

$$H^* + O_2 \Leftrightarrow OH^* + O^* \quad (R5)$$

$$O^* + H_2 \Leftrightarrow OH^* + H^* \quad (R6)$$

The preignition chemistry of methane is initiated primarily by reaction (R1). At high pressures or in the initial stages of hydrocarbon oxidation, high concentrations of HO_2 can initiate reaction (R2) [45]. When reaction (R1) is the dominant initiation step, reactions (R3) and (R4) may participate in further radical growth. Initiation reactions also involve the dissociation of H_2 and O_2 and reactions between H_2 and O_2. For example, the chain-branching reactions (R5) and (R6) are initiated by the production of H^* from these initiation reactions. Under supercharged engine conditions, CO reacts with HO_2, producing CO_2 and OH^*. Thus, CO oxidation at high pressures can be modelled by adding reaction (R2) to the syngas kinetics mechanism, as shown by Kim et al. [46].

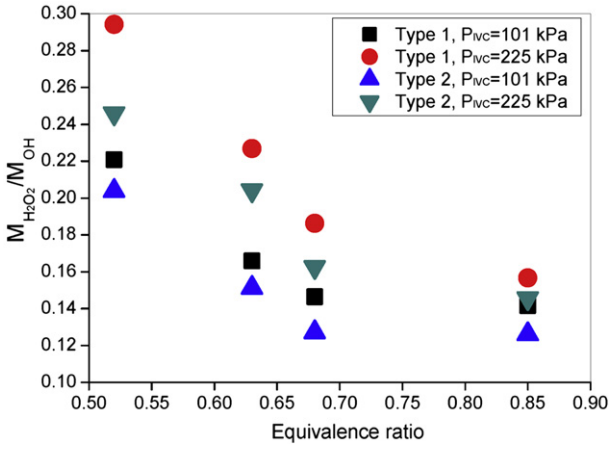

Fig. 2 – Relation between H_2O_2 and OH at engine naturally aspirated and supercharged conditions. T_{IVC} = 450 K.

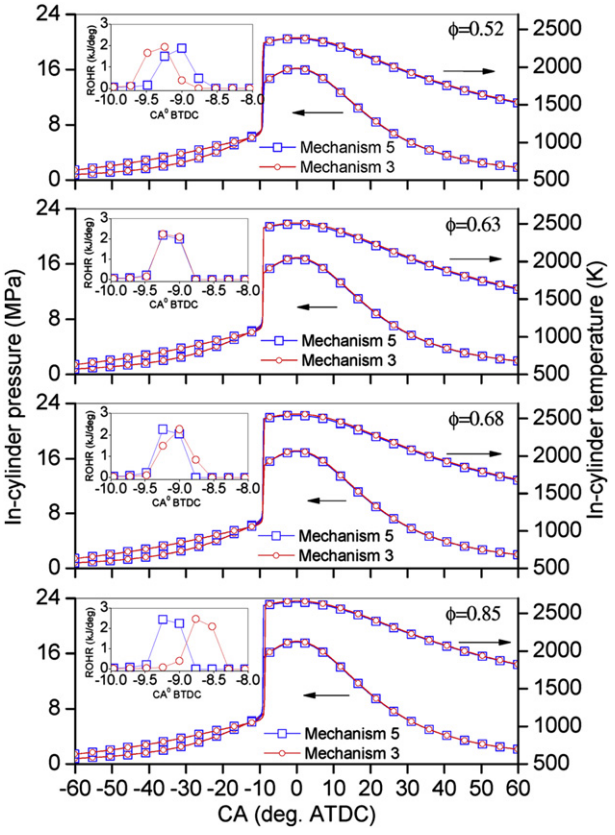

Fig. 3 – Comparison of in-cylinder pressure, temperature and heat release rate for mechanisms 3 and 5. Syngas Type 1, P_{IVC} = 225 kPa, T_{IVC} = 450 K.

4. Results and discussion

4.1. The effect of the $H_2O_2(+M) \Leftrightarrow OH^* + OH^*(+M)$ reaction

To clarify the effect of pressure on H_2O_2 formation during combustion under supercharged engine conditions, the H_2O_2/OH^* ratio was determined for two types of syngas at different equivalence ratios. Fig. 2 shows that for cases with higher pressures at IVC, the H_2O_2 concentration during combustion is usually higher than that at lower pressures. This is because at higher pressures, the high concentration of the mixture, including enhanced third-body efficiencies M, leads to a sufficient concentration of HO_2, which is less reactive than other free radicals, forming H_2O_2. Before high temperatures are reached, the characteristic reaction time of H_2/CO mixtures is long [33]. This reduction in reaction sensitivity causes the H_2O_2 concentration to increase. As the equivalence ratio increases, the H_2O_2/OH^* ratio gradually decreases, as does the difference between the H_2O_2/OH^* values at lower and higher pressures. This decrease is due to the enhanced decomposition of H_2O_2 and the increased chain-branching reaction rates at higher temperatures caused by the increase in the equivalence ratio. The figure also shows that the H_2O_2/OH^* ratio is lower for Type 2 syngas, which has a higher initial H_2 concentration. The higher initial H_2 concentration provides an enhanced chain-initiation process ensuring the occurrence of subsequent chain-branching reactions along with an increase in the OH^* concentration.

Because the $H_2O_2(+M) \Leftrightarrow OH^* + OH^*(+M)$ reaction during combustion provides access to a series of important

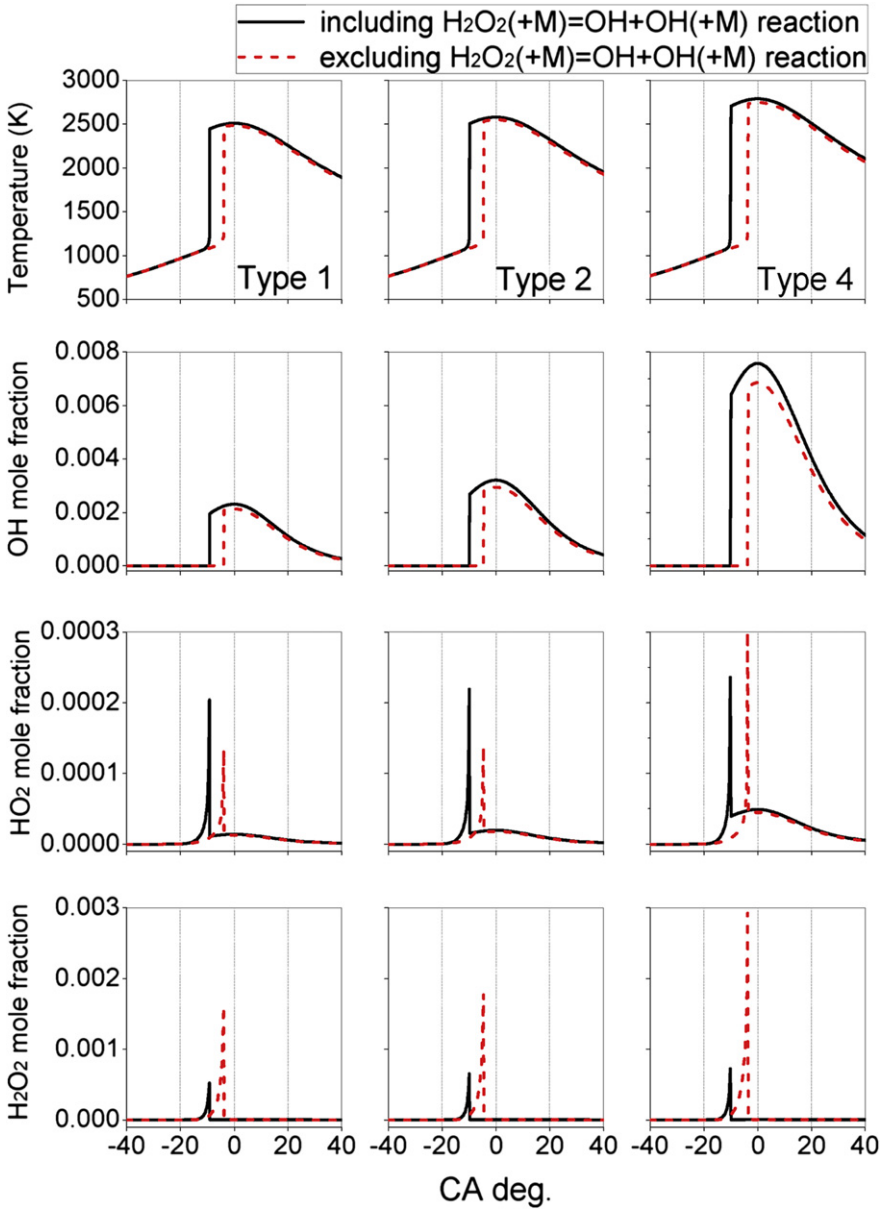

Fig. 4 – The effect of $H_2O_2(+M) = OH + OH(+M)$ reaction on in-cylinder temperature and mole fraction of intermediate species during combustion. P_{IVC} = 225 kPa, T_{IVC} = 450 K, ϕ = 0.63.

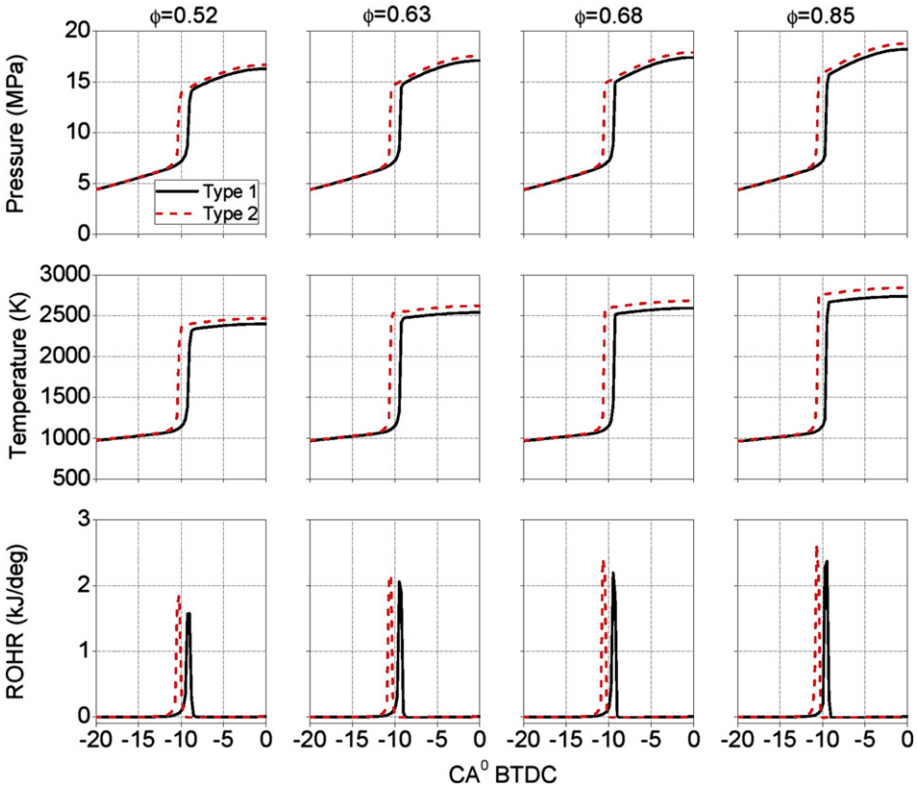

Fig. 5 – Effect of initial H_2 concentration on in-cylinder pressure, temperature and the rate of heat release. P_{IVC} = 225 kPa, T_{IVC} = 450 K.

secondary reactions, such as $OH^* + H_2O_2 \Leftrightarrow HO_2 + H_2O$, $HO_2 + HO_2 \Leftrightarrow H_2O_2 + O_2$, and $OH^* + HO_2 \Rightarrow H_2O + O_2$ [47], a chemical kinetics analysis was performed using mechanism 3 under supercharged conditions to determine the effect of this linking reaction on the combustion process. Two cases were computed, including and excluding this reaction from the reaction mechanism for Types 1, 2, and 4 syngas. The validity of using mechanism 3 for this type of analysis was confirmed by comparing the results at the same conditions with those of mechanism 5, GRI Mech 3.0. The results of cylinder pressure, temperature, and rate of heat release (ROHR) of mechanism 3 showed good agreement with those of mechanism 5, as shown in Fig. 3.

Fig. 4 shows the in-cylinder temperature and intermediate species formation computed by including and excluding the $H_2O_2(+M) \Leftrightarrow OH^* + OH^*(+M)$ reaction from the reaction mechanism. Although the in-cylinder temperatures were almost the same, the H_2O_2 exclusion led to an increased ignition delay. The reaction $H_2O_2(+M) \Leftrightarrow OH^* + OH^*(+M)$ provides access to a series of reactions producing very reactive OH^* radicals. Excluding this reaction from the mechanism suppresses the reactivity of the mixture and increases the ignition delay. As the H_2 initial concentration increased (from Type 1 to Type 4 syngas), the peak temperature also increased, as did the OH^* concentration. The H_2O_2 concentration also increased for the case without the $H_2O_2(+M) \Leftrightarrow OH^* + OH^*(+M)$ reaction. This can be explained by the fact that when this reaction is eliminated from the mechanism, the reaction path progresses through the $H_2O_2 + H^* \Leftrightarrow HO_2 + H_2$ and $H_2O_2 + O_2 \Leftrightarrow HO_2 + HO_2$ reactions. Therefore, HO_2 reacting with itself and with H_2 and OH^* radicals is reduced,

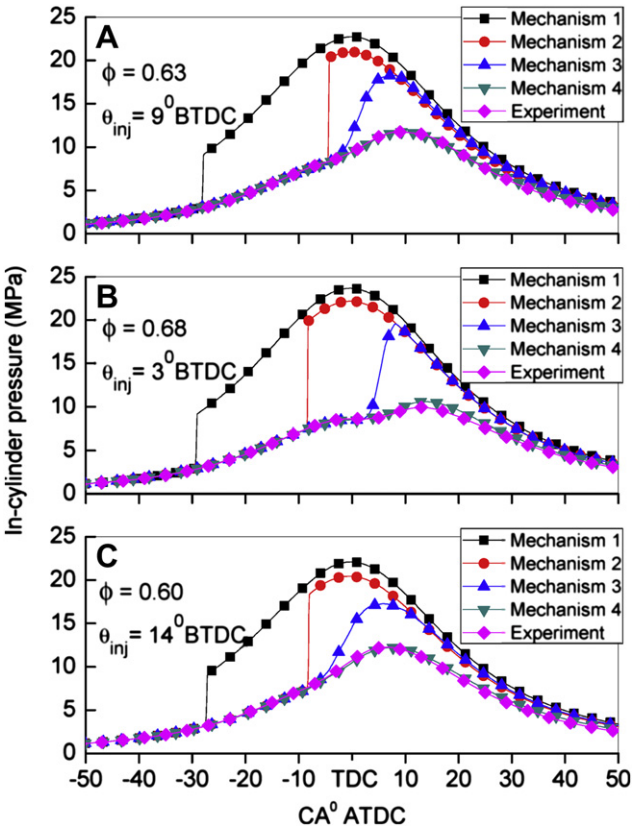

Fig. 6 – Comparison of CFD pressure data of all constructed mechanisms with experiment. (A) Type 1, (B) Type 2, (C) Type 3.

producing additional H_2O_2 species that cannot quickly decompose into OH* due to the missing linking reaction $H_2O_2(+M) \Leftrightarrow OH^* + OH^*(+M)$. At extremely high temperatures (over 2800 K) and at very high H_2/CO ratios, for reactions between H_2 and O_2, the thermal dissociation of H_2 has a significant effect on the chain-initiation reaction, such as $H_2 + O_2 \Rightarrow H^* + HO_2$, with further recombination of H and O atoms and OH* radicals producing higher concentrations of HO_2. A similar trend was observed for cases with different equivalence ratios considered in this work. Fig. 5 shows that a higher initial concentration of H_2 can induce earlier ignition as well as an increased ROHR. The ROHR increased with the equivalence ratio.

4.2. *Three-dimensional CFD combustion analysis*

To validate the mechanism for the in-cylinder-like conditions in a dual-fuel engine, an analysis was performed by applying

Table 4 – Constructed kinetics mechanism of syngas combustion for dual-fuel engine simulation (A units cal-cm-sec-K, E units cal/mol).

Reaction	A	n	E	Reference
n-Heptane reaction				
R1. $C_7H_{16} + 11O_2 \Leftrightarrow 7CO_2 + 8H_2O$	0.00	0.00	0.0	[41]
Eddy Break-up reaction $A_{ebu} = 4.0$; $B_{ebu} = 0.0$; $IOP = 1.0$; $f_i = 0.0$				
CH_4 reactions				
R2. $CH_4 + O_2 \Leftrightarrow CH_3 + HO_2$	3.98×10^{13}	0.00	56855.5	[39]
R3. $CH_4 + HO_2 \Leftrightarrow CH_3 + H_2O_2$	9.04×10^{12}	0.00	24629.4	[39]
R4. $CH_4 + OH \Leftrightarrow CH_3 + H_2O$	1.60×10^{7}	1.83	2771.1	[39]
R5. $CH_3 + O_2 \Leftrightarrow CH_2O + OH$	3.30×10^{11}	0.00	8934.4	[39]
R6. $CH_2O + OH \Leftrightarrow HCO + H_2O$	3.90×10^{10}	0.89	406.1	[39]
H_2 reactions				
R7. $H + O_2 \Leftrightarrow OH + O$	3.52×10^{16}	- 0.70	17061.4	[40]
R8. $H_2 + O \Leftrightarrow OH + H$	5.06×10^{4}	2.67	6287.6	[40]
R9. $H_2 + OH \Leftrightarrow H_2O + H$	1.17×10^{9}	1.30	3633.5	[40]
R10. $H + O_2 + M \Rightarrow HO_2 + M$	5.75×10^{19}	- 1.40	0.0	[40]
Enhanced third-body efficiencies: $H_2O = 18.0$, $H_2 = 2.50$, $O_2 = 0.0$, $CO = 1.20$, $CO_2 = 2.40$, $AR = 0.80$, $N_2 = 1.26$				
R11. $H + H + M \Rightarrow H2 + M$	1.30×10^{18}	- 1.00	0.0	[40]
Enhanced third-body efficiencies: $H_2O = 12.00$, $H_2 = 2.50$, $CO = 1.90$, $CO_2 = 3.80$, $AR = 0.50$				
R12. $H + OH + M \Rightarrow H_2O + M$	4.00×10^{22}	- 2.00	0.0	[40]
Enhanced third-body efficiencies: $H_2O = 16.00$, $H_2 = 2.00$, $CO_2 = 1.90$				
R13. $HO_2 + H \Rightarrow OH + OH$	7.08×10^{13}	0.00	293.8	[40]
R14. $HO_2 + H \Rightarrow H_2 + O_2$	1.66×10^{13}	0.00	821.8	[40]
R15. $HO_2 + OH \Rightarrow H_2O + O_2$	2.89×10^{13}	0.00	−496.9	[40]
R16. $H_2O_2 + H \Leftrightarrow H_2 + HO_2$	6.02×10^{13}	0.00	7950.0	[22]
R17. $OH + OH(+M) \Leftrightarrow H_2O_2(+M)$	7.40×10^{13}	- 0.37	0.0	[22]
Low-pressure limit:	2.30×10^{18}	- 0.90	- 1700.0	
Troe parameters: 0.7346, 94.0, 1756.0, 5182.0				
Enhanced third-body efficiencies: $H_2O = 6.00$, $H_2 = 2.00$, $CO = 1.50$, $CO_2 = 2.00$				
CO/CO_2 reactions				
R18. $CO + O(+M) \Leftrightarrow CO_2(+M)$	9.64×10^{10}	0.00	3800.0	[22]
Low-pressure limit:	2.07×10^{26}	- 3.34	7610.0	
Enhanced third-body efficiencies: $H_2O = 12.00$, $H_2 = 2.00$, $CO = 1.50$, $CO_2 = 2.00$				
R19. $CO + OH \Leftrightarrow CO_2 + H$	9.60×10^{11}	0.14	7352.0	[22]
DUPLICATE				
R20. $CO + OH \Leftrightarrow CO_2 + H$	7.32×10^{10}	0.03	−16.0	[22]
DUPLICATE				
R21. $CO + HO_2 \Leftrightarrow CO_2 + OH$	3.00×10^{13}	0.00	23000.0	[22]
R22. $CO + H_2O \Leftrightarrow CO_2 + H_2$	2.00×10^{11}	0.00	38000.0	[22]
R23. $HCO + M \Leftrightarrow CO + H + M$	1.20×10^{17}	−1.00	17000.0	[22]
Enhanced third-body efficiencies: $H_2O = 5.00$, $CO_2 = 3.00$, $H_2 = 1.90$, $CO = 1.90$				
R24. $HCO + O \Leftrightarrow CO_2 + H$	3.00×10^{13}	0.00	0.0	[22]
R25. $HCO + H \Leftrightarrow H_2 + CO$	1.00×10^{14}	0.00	0.0	[22]
R26. $HCO + OH \Leftrightarrow H_2O + CO$	5.00×10^{13}	0.00	0.0	[22]
R27. $HCO + HO_2 \Leftrightarrow H_2O_2 + CO$	4.00×10^{11}	0.00	0.0	[22]
R28. $HCO + HO_2 \Rightarrow H + OH + CO_2$	3.00×10^{13}	0.00	0.0	[22]
R29. $O_2 + CO \Leftrightarrow CO_2 + O$	2.53×10^{12}	0.00	47700.0	[22]
R30. $O_2 + HCO \Leftrightarrow HO_2 + CO$	1.00×10^{12}	0.00	0.0	[22]

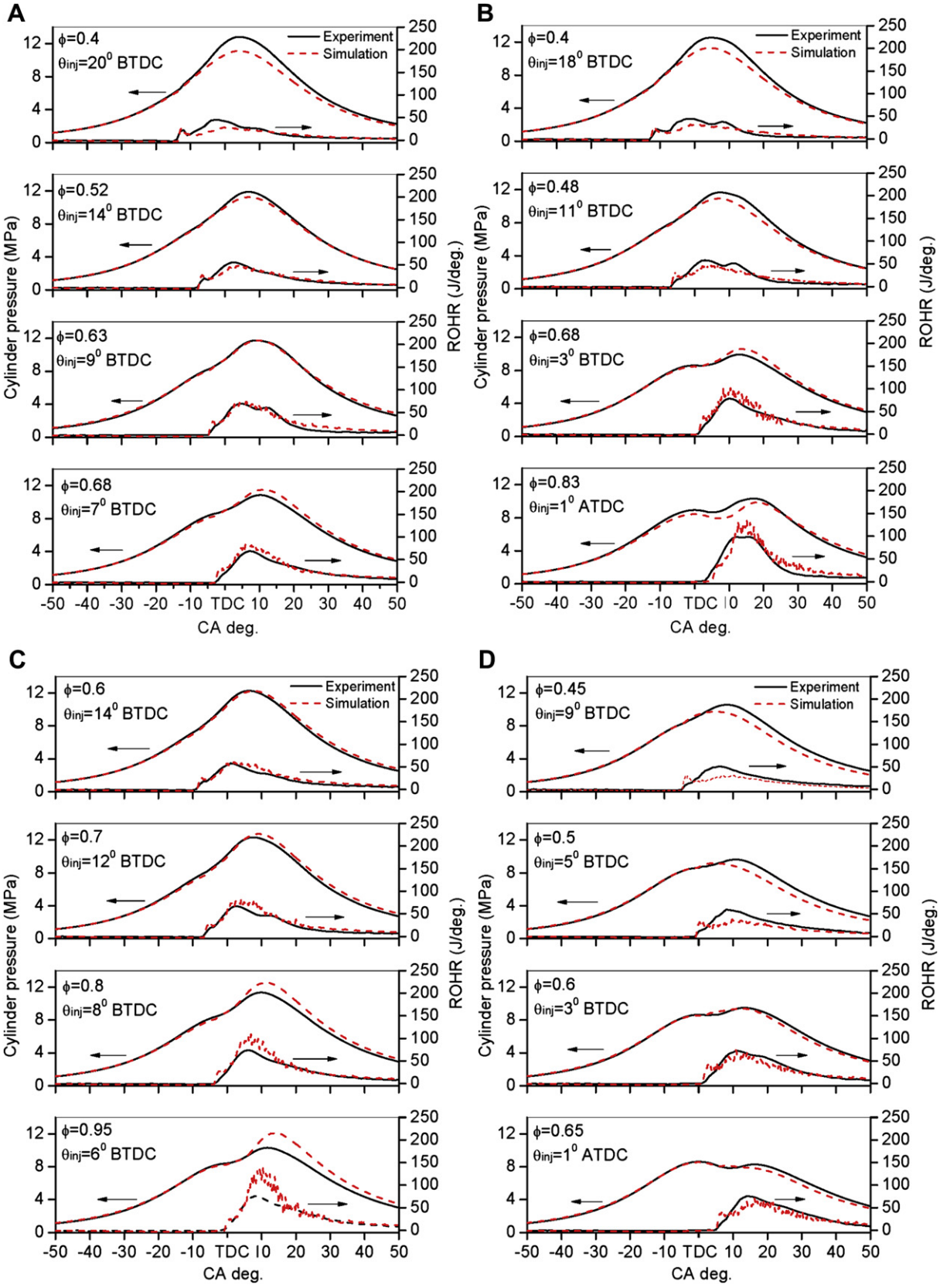

Fig. 7 – Comparison of experimental and simulated in-cylinder pressures and heat release rates. Computed using 3D-CFD with constructed mechanism 4. (A) Type 1, (B) Type 2, (C) Type 3, (D) Type 4. P_{IVC} = 225 kPa, T_{IVC} = 330 K.

a pilot injection using the coupled CFD and syngas chemical kinetics mechanism. Fig. 6 compares the simulated pressure data for all constructed mechanisms used in this study (mechanisms 1–4) with experimental pressure data. The in-cylinder pressure data of constructed mechanism 4 gave the best fit with the experimental results. A similar trend was observed for different equivalence ratios. Therefore, the final constructed mechanism 4, shown in Table 4, was further used for CFD analysis to simulate dual-fuel combustion for the different types of syngas given in Table 2. The pressure and ROHR plots shown in Fig. 7 show a good match between the simulation results and experimental data for different types of syngas at various equivalence ratios and injection timings. Fig. 8(A) and (B) compares the simulated mean in-cylinder temperature with the temperature from experiments calculated based on the ideal gas law. The temperature traces at different equivalence ratios were well correlated with the H_2 fraction consumed during the combustion. At lower equivalence ratios, the peak in-cylinder temperatures were lower compared with those at higher equivalence ratios. The same figure also shows that at lower equivalence ratios, the H_2 consumption decreased, whereas at higher equivalence ratios, the H_2 consumption increased. This trend was well correlated with the experimental data shown in Fig. 9. Higher levels of HC and CO, which is an indication of incomplete combustion, occur at lower equivalence ratios; the levels of HC and CO gradually decreased as the equivalence ratio increased. This trend was monitored for both Types 1 and 2 syngas, with lower HC and CO values for Type 2. The decrease was due to more complete combustion caused by the slightly higher in-cylinder temperature induced by the higher initial in-cylinder H_2 concentration. However, for Type 2 syngas at $\phi = 0.83$ and $\theta_{inj} = 1^\circ$ ATDC, the trend of the completeness of combustion did not match the experiment. In the experiment, at this condition, the HC and CO levels increased when diesel fuel was injected after TDC, as shown in Fig. 9. This was due to the decreased temperature and poor combustion after TDC. On the other hand, in the simulation, the combustion was almost completed, as predicted from the H_2 mass fraction trend because of the high rate of temperature rise, as shown in Fig. 8(B). This difference is related to the heat-transfer model. The thermal conditions inside the combustion chamber are closely tied to the mixture-burning rate and to the heat transfer from the hot gas to the cylinder walls. Thus, an appropriate heat-transfer correlation should be used to accurately predict the thermal conditions inside the cylinder in cases when combustion starts before TDC versus after TDC. This will be considered in future studies.

Fig. 10 shows the in-cylinder temperature and OH* concentration distribution. The OH* concentration built up as

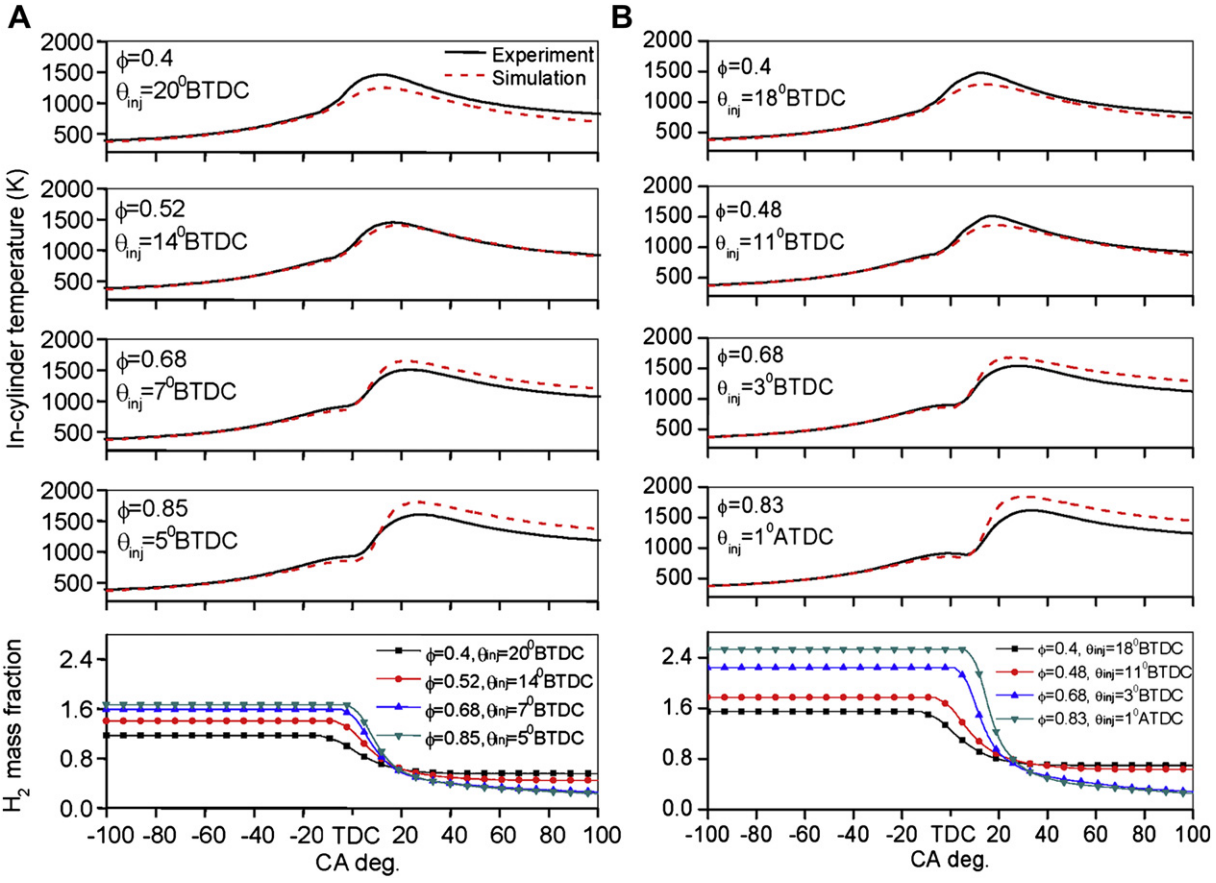

Fig. 8 – Comparison of experimental and simulated in-cylinder temperatures. The trend in H_2 consumption at different equivalence ratios. Computed using 3D-CFD with constructed mechanism 4. (A) Type 1, (B) Type 2. $P_{IVC} = 225$ kPa, $T_{IVC} = 330$ K.

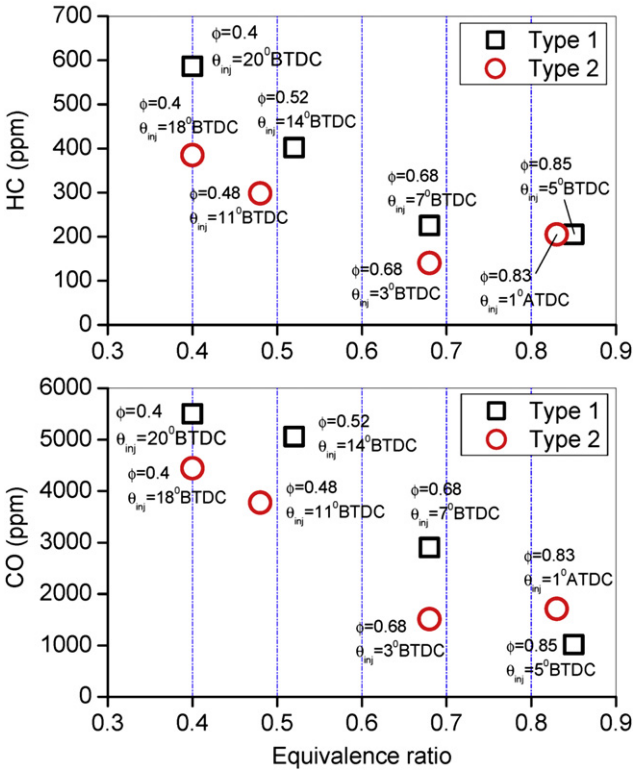

Fig. 9 – Experimental trend in HC and CO at different equivalence ratios for syngas of Type 1 and Type 2.

the temperature started to rise. As temperature rose, the flame front moved towards the cylinder wall, gradually consuming the unburned in-cylinder mixture. The highest spatial concentration of the built-up OH* was observed between the instance of ignition and 5° CA ATDC, which corresponds to the peak of the OH*curve.

To estimate the contribution of the chain-initiation and chain-propagation reactions of mechanism 4 to the heat production, the heat of reaction was computed for Types 1 and 2 syngas at different equivalence ratios using the CHEMKIN code. Fig. 11(A) shows that reaction (R1) was exothermic, and at high temperatures, this reaction became an important chain-initiating route to radical formation. However, high endothermicity of this reaction at low temperatures has also been reported [48]. Due to a higher initial fraction of H_2 in the Type 2 syngas composition, compared with that of Type 1, the heat-production rate of reaction (R1) occurred earlier for Type 2. The peak heat-production rate of reaction (R1) for Type 2 syngas was lower than that for Type 1 due to the lower temperature at which the heat was released. Increasing the cylinder temperature produced an increased flux of HO_2 radicals via reaction (R2). In turn, HO_2 recombined into H_2O_2 through reaction (R3), followed by thermal decomposition of H_2O_2 into OH* through reaction (R4), as shown in Fig. 11(B). Therefore, high exothermic reactions (R1) and (R2) were moderated by endothermic reactions (R3) and (R4).

The heat-production rate for Type 2 syngas at $\phi = 0.85$ showed a very different and unexpected trend; with the rapid release of heat for reactions (R1) and (R2) and rapid absorption of heat for reactions (R3) and (R4), as shown in Fig. 11(A) and (B). We suppose that this was due to a limitation of the constructed mechanism. Therefore, this mechanism can accurately predict the syngas combustion process only under lean conditions for equivalence ratios below 0.8, which was the primary objective of this study. In future studies, this constructed mechanism will be extended to a wider range of equivalence ratios and complemented with the reduced mechanism for NO_x chemistry.

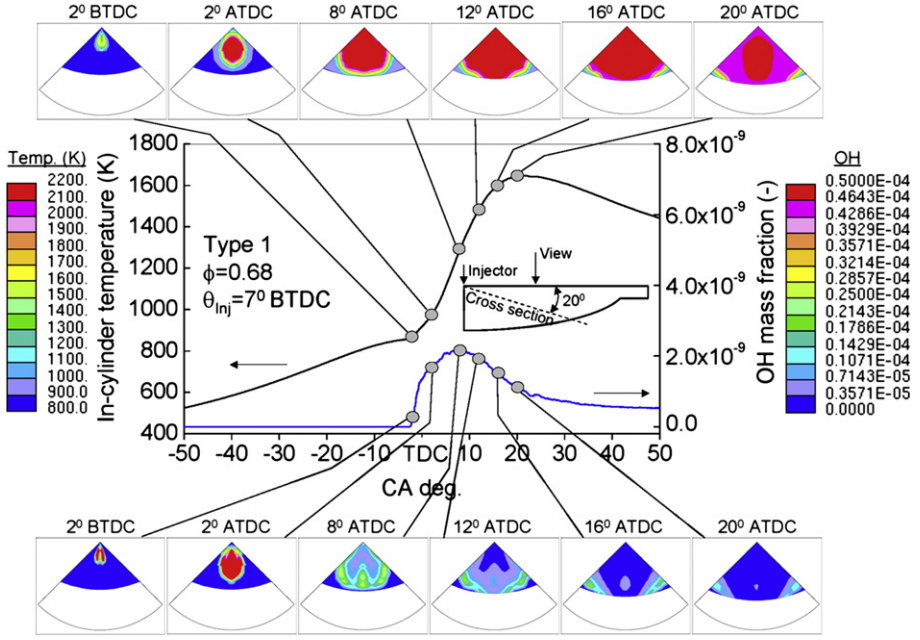

Fig. 10 – Mean volume-averaged and spatially-distributed in-cylinder temperature and OH concentration. P_{IVC} = 225 kPa, T_{IVC} = 330 kPa. Cross-section plane of a sector mesh is cut through the pilot fuel spray axis.

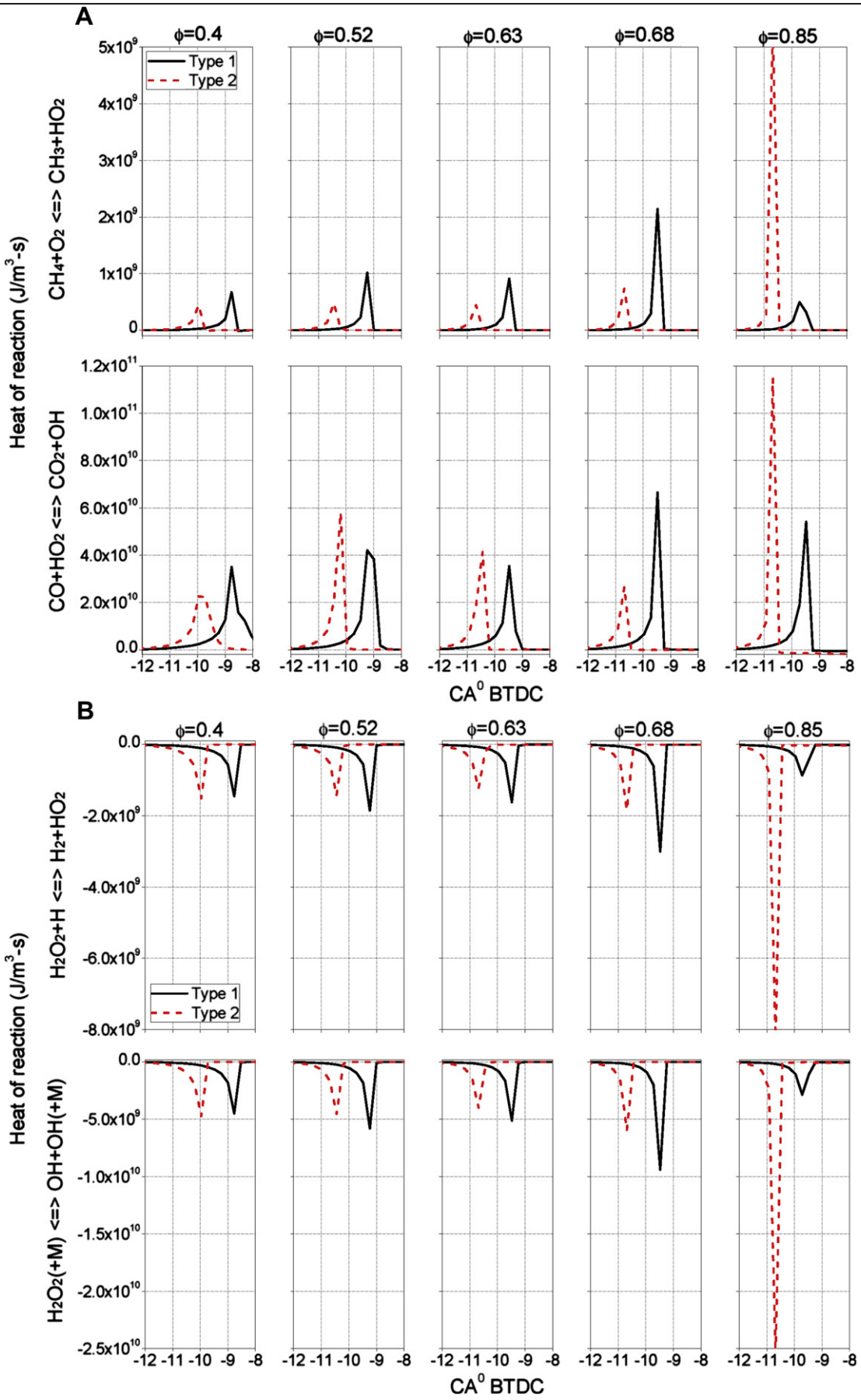

Fig. 11 – Heat of reaction for selected (A) chain-initiation and (B) chainpropagation reactions computed with the constructed mechanism 4. P_{IVC} = 225 kPa, T_{IVC} = 450 K.

5. Conclusion

A simulation using a CFD code with a constructed syngas chemical kinetic mechanism was performed to evaluate syngas combustion in a supercharged dual-fuel engine with various syngas initial compositions under lean conditions. The constructed mechanism was validated concurrently by using a chemical kinetics code and a multidimensional CFD code, and the results were compared with experimental data of combustion in a supercharged dual-fuel engine. The present model predicted the engine performance well, including the cylinder pressure history, heat-release rate data with respect to syngas composition equivalence ratio, and injection timing. The results demonstrated that under supercharged engine conditions, the importance of H_2O_2-based reactions should not be underestimated. After evaluating the released heat for the chain-initiating and chain-propagating reactions, the best comparison of results with experimental data was obtained for equivalence ratios below 0.8. As the equivalence ratio increased above this level, the heat contribution from each reaction also changed, and results began to deviate from the experiment data. With further development, this model could become an effective simulation tool to capture engine performance variations due to changes in the initial air–fuel ratio and syngas composition.

Acknowledgements

The authors are grateful to the Japan Society for the Promotion of Science (JSPS) for providing partial funding for this work.

Appendix. Supplementary material

Supplementary material associated with this article can be found, in the online version, at doi:10.1016/j.ijhydene.2011.07.140.

REFERENCES

[1] Rao AD, Samuelssen GS, Robson FL, Geisbrecht RA. Power plant system configurations for the 21st century, vol. 1. ASME Int. Gas Turb Inst, Turbo Expo IGTI; 2002. 831.
[2] Wang L, Weller CL, Jones DD, Hanna MA. Contemporary issues in thermal gasification of biomass and its application to electricity and fuel production. Biomass Bioenergy 2008;32:573–81.
[3] Shilling NZ, Lee DT. IGCC-clean power generation alternative for solid fuels: GE power systems. PowerGenAsia; 2003.
[4] Sridar G, Paul PJ, Mukunda HS. Biomass derived producer gas as a reciprocating engine fuel-an experimental analysis. Biomass Bioenergy 2001;21:61–72.
[5] Shudo T, Takahashi T. Influence of reformed gas composition on HCCI combustion engine system fueled with DME and H_2–CO–CO_2 which are onboard-reformed from methanol utilizing engine exhaust heat. Trans JSME B 2004;70:2663–9.
[6] Shudo T. An HCCI combustion engine system using on-board reformed gases of methanol with waste heat recovery: ignition control by hydrogen. Int J Vehicle Design 2006;41:206–26.
[7] Li H, Karim GA. Exhaust emissions from an SI engine operating on gaseous fuel mixtures containing hydrogen. Int J Hydrogen Energy 2005;30:1491–9.
[8] Karim GA. Combustion in gas fueled compression: ignition engines of the dual fuel type. J Eng Gas Turb Power 2003;125:827–36.
[9] Liu Z, Karim GA. Simulation of combustion processes in gas-fuelled diesel engine. J Power Energy 1997;211:159–69.
[10] Poonia MP, Ramesh A, Gaur RR. Effect of intake air temperature and pilot fuel quantity on the combustion characteristics of a LPG-diesel dual-fuel engine. SAE paper, 982455.
[11] Karim GA, Moore NPW. The production of hydrogen by the partial oxidation of methane in a dual-fuel engine. SAE paper, 901501.
[12] Karim GA, Wierzba I. Safety measures associated with the operation of engines on various alternative fuels. Reliability Eng Syst Saf 1992;37:93–8.
[13] McMillian MH, Lawson SA. Experimental and modeling study of hydrogen/syngas production and particulate emissions from a natural gas-fuelled partial oxidation engine. Int J Hydrogen Energy 2006;31:847–60.
[14] Bilcan A. Contribution to the study of the thermodynamic cycle of dual-fuel. PhD thesis 2003, Nantes University, France.
[15] Baratieri M, Baggio P, Bosio P, Grigiante M, Longo GA. The use of biomass syngas in IC engines and CCGT plants: a comprehensive analysis. Appl Therm Eng 2009;29:3309–18.
[16] Boehman AL, Le Corre O. Combustion of syngas in internal combustion engines. Combust Sci Tech 2008;180:1193–206.
[17] Tomita E, Fukatani N, Kawahara N, Maruyama K, Komoda T. Combustion characteristics and performance of supercharged pyrolysis gas engine with micro-pilot ignition. CIMAC congress 2007, Paper No. 178.
[18] Roy MM, Tomita E, Kawahara N, Harada Y, Sakane A. Performance and emission comparison of a supercharged dual-fuel engine fueled by producer gases with varying hydrogen content. Int J Hydrogen Energy 2009;34:7811–22.
[19] Roy MM, Tomita E, Kawahara N, Harada Y, Sakane A. Performance and emissions of a supercharged dual-fuel engine fueled by hydrogen-rich coke oven gas. Int J Hydrogen Energy 2009;34:9628–38.
[20] Yetter RA, Dryer FL, Rabitz H. A comprehensive reaction mechanism for carbon monoxide/hydrogen/oxygen kinetics. Combust Sci Tech 1991;79:97.
[21] Saxena P, Williams FA. Testing a small detailed chemical-kinetic mechanism for the combustion of hydrogen and carbon monoxide. Combust Flame 2006;145:316–23.
[22] Frassoldati A, Faravelli T, Ranzi E. The ignition, combustion and flame structure of carbon monoxide/hydrogen mixtures. Note 1: detailed kinetic modeling of syngas combustion also in presence of nitrogen compounds. Int J Hydrogen Energy 2007;32:3471–85.
[23] Cuoci A, Frassoldati A, Buzzi Ferraris G, Faravelli T, Ranzi E. The ignition, combustion and flame structure of carbon monoxide/hydrogen mixtures. Note 2: fluid dynamics and kinetic aspects of syngas combustion. Int J Hydrogen Energy 2007;32:3486–500.
[24] Liu C, Karim GA. A simulation of the combustion of hydrogen in HCCI engines using a 3D model with detailed chemical kinetics. Int J Hydrogen Energy 2008;33:3863–75.
[25] Wang Y, Zhang X, Li C, Wu J. Experimental and modeling study of performance and emissions of SI engine fuelled by natural gas-hydrogen mixtures. Int J Hydrogen Energy 2010;35:2680–3.

[26] Slavinskaya N, Braun-Unkhoff M, Frank P. Reduced reaction mechanisms for methane and syngas combustion in gas turbines. J Eng Gas Turb Power 2008;130(021504):1–6.
[27] Starik AM, Titova NS, Sharipov AS, Kozlov VE. Syngas oxidation mechanism. Combust Expl Shock Waves 2010;46: 491–506.
[28] Sun H, Yang SI, Jomaas G, Law CK. High-pressure laminar flame speeds and kinetic modeling of carbon monoxide/ hydrogen combustion. Proc Combust Inst 2007;31:439–46.
[29] Sivaramakrishnan R, Comandini A, Tranter RS, Brezinsky K, Davis SG, Wang H. Combustion of CO/H_2 mixtures at elevated pressures. Proc Combust Inst 2007;31:429–37.
[30] Cavaliere DE, De Ioannon M, Sabia P, Allegorico M, Marchione T, Sirignano M, et al. A comprehensive kinetic modeling of ignition of syngas/air mixtures at low temperatures and high pressures. Combustion Colloquia 2009, 32nd Meeting on Combustion of the Italian Section of the Combustion Institute, April 26–28, Napoli, University Federico II, 26-28 of April, 2009.
[31] Smith GP, Golden DM, Frenklach M, Moriarty NW, Eiteneer B, Goldenberg M, et al. GRI-Mech home page http://www.me.berkeley.edu/gri_mech/.
[32] Mittal G, Sung CJ, Fairweather M, Tomlin AS, Griffiths JF, Hughes KJ. Significance of the HO_2 + CO reaction during the combustion of CO + H_2 mixtures at high pressures. Proc Combust Inst 2007;31:419–27.
[33] Chaos M, Fryer FL. Syngas combustion kinetics and applications. Combust Sci Tech 2008;180:1053–96.
[34] Papagiannakis RG, Rakopoulos CD, Hountalas DT, Giakoumis EG. Study of the performance and exhaust emissions of a spark-ignited engine operating on syngas fuel. Int J Altern Propulsion 2007;1:190–215.
[35] Gamino B, Aguillon J. Numerical simulation of syngas combustion with a multi-spark ignition system in a diesel engine adapted to work at the Otto cycle. Fuel 2010;89: 581–91.
[36] Kong SC, Reitz RD. Use of detailed chemical kinetics to study HCCI engine combustion with consideration of turbulent mixing effects. J Eng Gas Turb Power 2002;124:702–7.
[37] Reitz RD, Diwakar R. Effect of drop breakup on fuel sprays. SAE paper, 860469.
[38] Reitz RD, Diwakar R. Structure of high-pressure fuel spray. SAE paper, 870598.
[39] Li SC, Williams FA. A reduced reaction mechanism for predicting knock in dual-fuel engines. SAE paper 2000-01-0957.
[40] Fernandez-Galisteo D, del Alamo G, Sanchez AL, Linan A. Zeldovich analysis of hydrogen-air premixed flames. In: Proceedings of the Europian Combustion Meeting 2007.
[41] Methodology, Star-CD V4.0, pp. 10–5, Cd-Adapco Inc.
[42] Donkerbroek AJ, van Vliet AP, Somers LMT, Frijters PJM, Klein-Douwel RJH, Dam NJ, et al. Time- and space-resolved quantitative LIF measurements of formaldehyde in a heavy-duty diesel engine. Combust Flame 2010;157:155–66.
[43] Fernandez-Galisteo D, Sanchez AL, Linan A, Williams FA. One-step reduced kinetics for lean hydrogen-air deflagration. Combust Flame 2009;156:985–96.
[44] Mittal G, Sung CJ, Yetter RA. Autoignition of H_2/CO at elevated pressures in a rapid compression machine. Int J Chem Kinet 2006;38:516–29.
[45] Law CK. Combustion physics. Cambridge University Press; 2006.
[46] Kim TJ, Yetter RA, Dryer FL. New results on CO oxidation: high pressure, high temperature experiments and comprehensive kinetic modeling. Proc Combust Inst 1994;25: 759–66.
[47] Kappel C, Luther K, Troe J. Shock wave study of the unimolecular dissociation of H_2O_2 in its falloff range and of its secondary reactions. Phys Chem Chem Phys 2002;4: 4392–8.
[48] Gardiner WC. Gas-phase combustion chemistry. New York: Springer–Verlag; 2000.